Journal of Materials Chemistry B

PAPER

View Article Online
View Journal | View Issue

Cite this: J. Mater. Chem. B, 2018, 6, 2630

Organic nanoparticles with ultrahigh quantum yield and aggregation-induced emission characteristics for cellular imaging and real-time two-photon lung vasculature imaging

Jie Liu,[a] Maximilien Evrard,[b] Xiaolei Cai,[a] Guangxue Feng,[a] Nikodem Tomczak,[c] Lai Guan Ng[b] and Bin Liu *[abc]

Received 8th February 2018,
Accepted 3rd April 2018

DOI: 10.1039/c8tb00386f

rsc.li/materials-b

Fluorescent organic nanoparticles based on small molecules have emerged as an attractive class of fluorescent agents for bioimaging in recent years. Herein, we report orange light-emitting BTPEBD based organic nanoparticles (BTPEBD NPs) with a large Stokes shift (>135 nm), ultrahigh quantum yield (>90% in water) and aggregation-induced emission characteristics. Single nanoparticle analysis studied by wide field microscopy imaging further proves that the BTPEBD NPs exhibit high brightness and good photostability. Both *in vitro* and *in vivo* experiments reveal that the BTPEBD NPs are promising fluorescent agents for cellular imaging and real-time two-photon lung vasculature imaging.

Introduction

Fluorescent nanoparticles (NPs) are an attractive class of fluorescent agents for bioimaging applications.[1–7] In comparison with inorganic fluorescent NPs, notably quantum dots (QDs), organic fluorescent NPs have received more attention in recent years due to their synthetic versatility and less cytotoxicity concerns caused by heavy-metal release.[8,9] Moreover, organic NPs can encapsulate large quantities of organic dyes,[10] exhibiting improved photostability compard to molecular organic dyes. For practical bioimaging applications, fluorescent NPs with sufficient brightness are desirable for high-contrast imaging. To yield high brightness, the ideal solution is to encapsulate as many dyes as possible in the organic NPs. However, when a large number of organic dye molecules is confined within a small space, weakened or even quenched fluorescence is often observed due to π–π stacking and/or the presence of other non-radiative pathways, a typical photophysical phenomenon for traditional organic dyes, which is notoriously known as aggregation-caused quenching (ACQ).[11] The ACQ effect has been a thorny hurdle in the fabrication of bright and photostable NPs.

Different from the traditional ACQ dyes, typical fluorogens with aggregation-induced emission (AIE) characteristics are almost non-fluorescent in a molecularly dissolved state, but could be induced to show high fluorescence in an aggregate state.[12–15] This unique feature of AIEgens offers a great opportunity to prepare organic NPs with high dye loading contents. As a result, the resultant AIE NPs exhibit exceptionally high brightness, large Stokes shift (>100 nm) and good biocompatibility,[16] which have been successfully utilized for cellular imaging,[17] long-term cell tracing,[18,19] *in vivo* tumour detection,[20–28] imaging-guided surgery,[29] and two-photon[30–34] and three-photon imaging.[35–37] For multi-photon applications, the NP brightness is calculated from the product of quantum yield (QY) and the absorption coefficient. Therefore, the straightforward strategy for brightness enhancement is to improve the QY or absorption cross-section.[38,39]

For *in vitro* and *in vivo* applications, organic nanoparticles with long wavelength emissions are highly desirable. One efficient strategy to yield AIEgens with long wavelength emission is to build molecules with donor–acceptor (D–A) structures.[16,20,21,27,32,40–43] An electron-deficient unit of benzothiadiazole (BT) has been widely employed to construct D–A structured AIEgens with emission from green to red.[30,33,44] On the other hand, 2,1,3-benzoxadiazole (BD) is similar to a BT unit by replacing the sulfur atom with an oxygen atom. Many commercially available derivatives of BD, such as 4-chloro-7-nitrobenzo-2,1,3-oxadiazole (NBD-Cl), have been widely employed as bright fluorescent probes.[45] In addition, some previous reports also revealed that 2,1,3-benzoxadiazole-containing conjugated polymers exhibited higher QY and larger absorption coefficient than benzothiadiazole-containing ones.[46–49]

In this contribution, we report the synthesis of 4,7-bis[4-(1,2,2-triphenylvinyl)phenyl]benzoxadiazole (BTPEBD) with AIE characteristics and the fabrication of BTPEBD NPs for cellular

[a] Department of Chemical and biomolecular Engineering, National University of Singapore, 4 Engineering Drive 4, 117585, Singapore. E-mail: cheliub@nus.edu.sg
[b] Singapore Immunology Network (SIgN), Agency for Science Technology and Research (A*STAR), Biopolis, 138648, Singapore
[c] Institute of Materials Research and Engineering (IMRE), Agency for Science Technology and Research (A*STAR), Fusionopolis, 138634, Singapore

imaging and two-photon lung vasculature imaging. Interestingly, the AIE NPs exhibit a high QY of 90% in water. We demonstrate at a single particle level that BTPEBD NPs have high brightness and good photostability. After evaluation of the cytotoxicity, *in vitro* cell imaging and *in vivo* two-photon lung vasculature imaging using BTPEBD NPs are demonstrated.

Results and discussion

Synthesis and characterization of BTPEBD

As shown in Fig. 1a, BTPEBD was designed with a donor–acceptor–donor (D–A–D) structure, in which a tetraphenylethene unit was employed as the electron donor and a benzoxadiazole unit was chosen as the electron acceptor. BTPEBD was readily synthesized in two steps starting from 1-(4-bromophenyl)-1,2,2-triphenylethylene **1**. In brief, **1** was treated with bis(pinacolato)diboron in the presence of potassium acetate and Pd(dppf)Cl_2 to offer the corresponding boric ester **2**, which was then reacted with 4,7-dibromo-2,1,3-benzoxadizole *via* a Suzuki-coupling reaction to yield BTPEBD in a total yield of 88% over two steps. The correct chemical structure of BTPEBD was verified by NMR and MS.

The absorption spectrum of BTPEBD in tetrahydrofuran (THF) is shown in Fig. 1b. The absorption band at around 310 nm is derived from π–π* and n–π* transitions of the conjugated aromatic segments and that at longer wavelength is attributed to the intramolecular charge transfer (ICT) from the donor (TPE) to acceptor (BD) unit. The absorptivity of BTPEBD at 426 nm is 1.35×10^4 M^{-1} cm^{-1}, indicative of good light-harvesting ability. The presence of ICT was confirmed by the calculated frontier orbitals, which was obtained by density functional theory (DFT) calculations using the Gaussian 03 suite of programs and a nonlocal density functional of B3LYP with 6-31G(d) basis. As shown in Fig. 1c, the highest occupied molecular orbital (HOMO) is localized mainly on the TPE axis while the lowest unoccupied molecular orbital (LUMO) is predominately on the benzoxadiazole axis. The difference in electron cloud distribution verifies its intrinsic ICT property.

The optical properties of BTPEBD were evaluated in THF/water mixtures. THF and water are a good solvent with low polarity and a poor solvent with high polarity for BTPEBD, respectively. Variation of their ratios enables fine-tuning of the solvent polarity and the aggregation extent of BTPEBD. As shown in Fig. 2a, BTPEBD in pure THF shows orange emission with an emission maximum at 563 nm. As the water fraction (f_w) is gradually increased from 0 to 60 vol%, a decrease in fluorescence intensity is observed, which is accompanied by a redshift from 563 to 590 nm, due to the twisted intramolecular charge transfer (TICT) effect. With further increased f_w, the fluorescence intensity increases significantly due to the aggregation formation, demonstrating their AIE characters. In addition, the emission maximum undergoes a blueshift from 563 to 552 nm when f_w changes from 60 vol% to 90 vol%. Such a blue shift was also observed in other D–A-structured AIE molecules, attributed to the TICT-to-local emission transition.[50] The fluorescence intensities of BTPEBD at $f_w > 70$ vol% are higher than that in pure THF solution (Fig. 2b). Fig. 2c shows photographs of BTPEBD in the mixtures of THF/water with varying f_w. As BTPEBD shows both TICT and AIE features, it has bright fluorescence in both less polar organic solvents and aggregated states.

Fabrication and characterization of BTPEBD NPs

To make the AIEgen compatible with aqueous media, BTPEBD was used to fabricate NPs using a modified nanoprecipitation method (Fig. 3a). In brief, a solution of BTPEBD, 1,2-distearoyl-*sn-glycero*-3-phosphoethanolamine-*N*-[methoxy(polyethylene glycol)-2000] (DSPE-PEG_{2000}) and 1,2-distearoyl-*sn-glycero*-3-phosphoethanolamine-*N*-[maleimide(polyethylene glycol)-2000] (DSPE-PEG_{2000}-Mal) dissolved well in THF was added into ten-fold of water under continuous sonication. After THF evaporation and filtration, the resultant BTPEBD NPs were obtained. BTPEBD NPs show excellent colloidal stability without any observable precipitation after being kept at 4 °C for over 3 months. Laser light scattering (LLS) study shows that BTPEBD has a mean

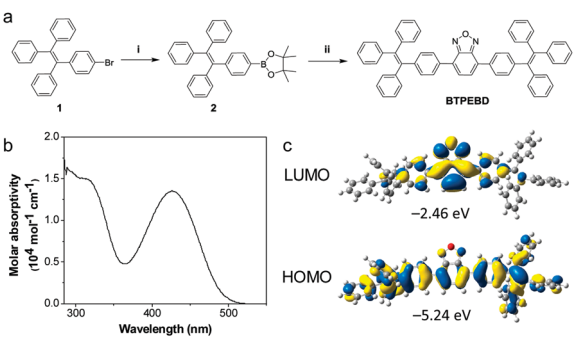

Fig. 1 (a) Synthetic route to BTPEBD. Reagents and conditions: (i) bis-(pinacolato)diboron, AcOK, Pd(dppf)Cl_2, dioxane, 85 °C, 20 h; (ii) 4,7-dibromo-2,1,3-benzoxadiazole, Pd(PPh_3)$_4$, potassium carbonate, tetrabutylammonium bromide, water/toluene, 90 °C, 2 days. (b) Absorption spectrum of BTPEBD in THF with a concentration of 1 μM. (c) Calculated molecular orbitals for BTPEBD.

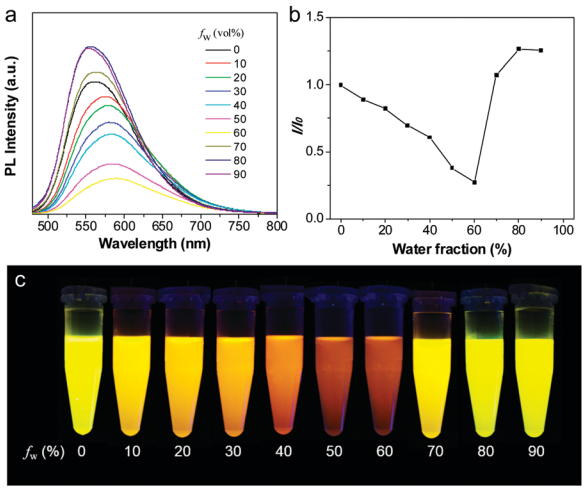

Fig. 2 Optical properties of BTPEBD in THF/water mixtures. PL spectral changes (a) and plot of the relative PL intensity (b) of BTPEBD in THF/water mixtures with different water fractions (f_w). I_0 and I are the PL intensities of BTPEBD in pure THF (f_w = 0) and a THF/water mixture with a specific f_w, respectively. (c) Photographs of BTPEBD in THF/water mixtures with different f_w.

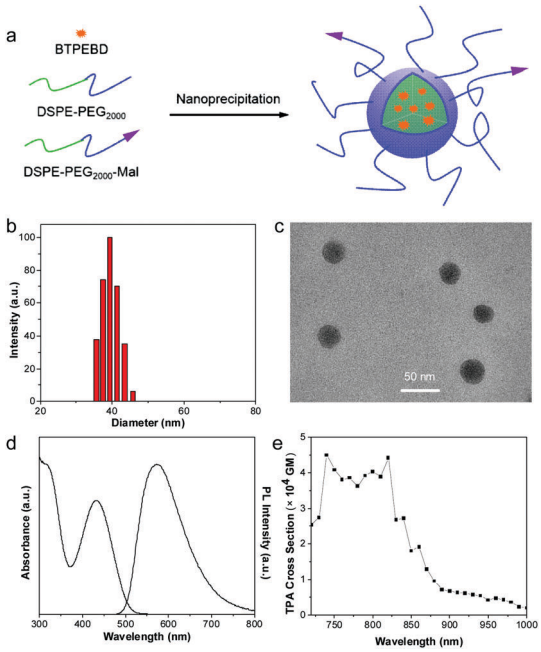

Fig. 3 (a) The schematic illustration of BTPEBD NP fabrication. (b) LLS and (c) TEM results of BTPEBD NPs. (d) UV-vis and PL spectra of BTPEBD NPs in water. (e) Two-photon absorption spectrum of BTPEBD in water.

diameter of 39 nm (Fig. 3b), which is slightly larger than that obtained from transmission electron microscopy (TEM, 32 nm) study (Fig. 3c), due to the shrinkage of the NPs in the dry state. BTPEBD NPs have an intense absorption peak at 436 nm with a tail extending to over 500 nm (Fig. 3c). In comparison with the absorption spectrum of BTPEBD in THF, the ICT-caused absorption band of BTPEBD NPs is red-shifted by 10 nm, indicating the presence of intermolecular interaction. BTPEBD NPs in water exhibit strong orange emission at 574 nm with an ultrahigh QY of 90%, which was determined by using 4-(dicyanomethylene)-2-methyl-6-(*p*-dimethylaminostyryl)-4*H*-pyran in methanol (QY = 43%) as a reference.[51] This is highly advantageous for obtaining high quality imaging. In addition, the two-photon absorption (TPA) spectrum of BTPEBD NPs was measured in water in the 720–1000 nm range at 10 nm intervals. As shown in Fig. 3e, the TPA cross section (δ) shows high values of up to ~44 900 GM in a wide range from 740 to 820 nm, using Rhodamine 6G in methanol as the standard. The maximum $\eta\delta$ was calculated to be ~40 400 GM, which is higher than many other reported organic dye loaded NPs in the literature.[31–34] These results indicate that BTPEBD NPs are good TPA probes.

Single particle fluorescence properties and photostability

As fluorescent labels for bioimaging applications, the final brightness of a single NP is one of the important properties to be evaluated. In this study, the brightness of a single BTPEBD NP was assessed by wide field microscopy imaging. To observe the fluorescence from a single BTPEBD NP, the NPs were immobilized on a glass cover slide from a dilute solution. Fig. 4a shows the wide field image of individual DTPEBD NPs, which was acquired upon excitation at 488 nm with fluorescence intensity collection over 100 s. Each white spot in the image represents a single BTPEBD NP. The BTPEBD images exhibit high contrast between the NPs and background, suggesting that it could be a good candidate for fluorescence imaging. Since there would be intensity variations among different BTPEBD NPs, it is logical to use statistical metrics to analyse the data. To this end, we have chosen 586 BTPEBD NPs for analysis. Fig. 4b is the histogram of the total photo counts emitted in 100 s from the BTPEBD NPs. On average, 1.10×10^6 counts were collected from each BTPEBD NP.

Apart from brightness, the stability of a single NP is also of vital importance for bioimaging applications, especially for tracking experiments and long-term imaging. It is well known that organic fluorescent molecules are not photochemically inert and their fluorescence intensity will ultimately gradually fade under high power continuous illumination due to stepwise photobleaching of the chromophores. To study the fading behaviour of a single BTPEBD NP, the fluorescence intensity was monitored before and after 100 s continuous illumination, which is plotted as Fig. 4c. The extent of the difference indicates the magnitude of photobleaching. A diagonal line was drawn for reference and would represent no change in intensity over 100 s. Any data point lying close to the diagonal line could be considered as without photobleaching, since intensity fluctuations were inevitable in these studies. It is observed that most of the data points lied close to the diagonal line, which reflects good stability of the BTPEBD NPs. Although some NPs become dimmer after continuous illumination, these fading NPs only made up roughly 10% of the total population. Representative intensity and time-traces of different BTPEBD NPs are shown in Fig. 4d, which further prove the good stability of the single particles.

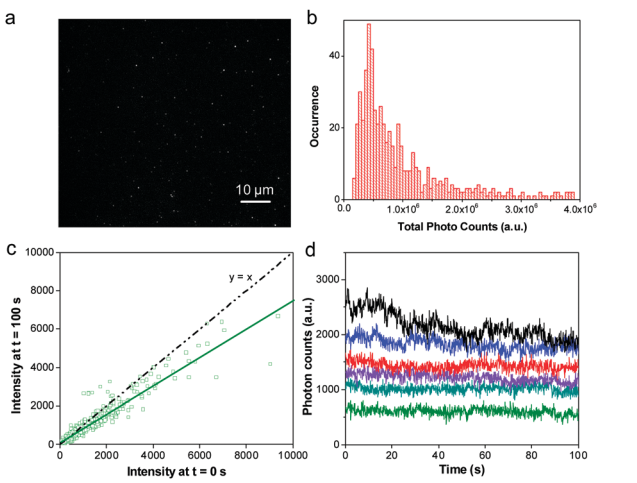

Fig. 4 (a) 76 × 76 μm^2 wide-field fluorescence images of single BEPTBD NPs immobilized on a glass cover slip. (b) Histogram of the total photo counts emitted during 100 s from BTPEBD NPs after ground subtraction. (c) Data points of individual BTPEBD NPs plotted on their initial intensity against final intensity. The points were fitted with a linear line. A diagonal line was drawn as a reference. (d) Representative intensity time-traces of single BTPEBD NPs.

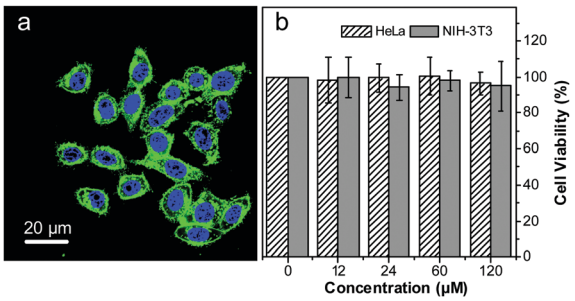

Fig. 5 (a) CLSM image of HeLa cells incubated with BTPEBD-Tat NPs at a concentration of 2 μM. Green emission is from BTPEBD NPs with E_x = 488 nm and E_m = 560–650 nm and blue emission is from DAPI with E_x = 405 nm and E_m = 430–450 nm. (b) Cell viabilities of HeLa and NIH-3T3 cells after incubation with BTPEBD NPs at various concentrations for 24 h.

Cell imaging and cytotoxicity

To demonstrate the capability of BTPEBD NPs in cellular imaging, we used BTPEBD NPs to stain HeLa cells. To enhance the cell uptake efficiency for BTPEBD NPs, Tat ligands were introduced on the NP surface *via* a click reaction to afford BTPEBD-Tat NPs. HeLa cells were incubated with BTPEBD-Tat NPs (2 μM) for 2 h followed by staining their nuclei with 4′,6-diamidino-2-phenylindole (DAPI). The confocal laser scanning microscopy (CLSM) image is shown in Fig. 5a. Bright green fluorescence in the cytoplasm around the nuclei was observed, indicating that the BTPEBD-Tat NPs can be efficiently taken-up by the HeLa cells with sufficient brightness. In addition, the cytotoxicity of the BTPEBD-Tat NPs was estimated by MTT assays (Fig. 5b). The cell viability remains over 90% after 24 h even at a high concentration of 120 μM, indicative of low cytotoxicity of the BTPEBD-Tat NPs for both cancer and normal cells.

Two-photon lung vasculature imaging

After illustrating the use of BTPEBD-Tat NPs as a cell-labelling reagent, we next studied whether such NPs could be utilized as vascular probes *in vivo*. To do so, 50 μg of BTPEBD NPs were administered to live mice, and the lung vasculature was imaged using a two-photon microscope. The experiments were performed upon excitation at 800 nm and the fluorescent signals were collected with a 525/50 longpass mirror. Fig. 6 shows the representative two-photon fluorescence images of the lung vasculature at various depths. It is observed that the major blood vessels and the smaller capillaries could be visualized with the help of BTPEBD NPs. Even at a depth higher than 20 μm, the vasculature can be visualized with a high resolution, demonstrating that BTPEBD NPs could act as excellent two-photon probes for *in vivo* imaging.

Experimental section

Preparation of nanoaggregates

The preparation of nanoaggregates mainly involves three steps: (i) a stock solution of BTPEBD in tetrahydrofuran (THF) was prepared with a concentration of 5×10^{-4} M; (ii) 50 μL of the stock solution was added to a 5 mL tube and diluted with appropriate amounts of THF; and (iii) appropriate amounts of water were added to the tube in one portion followed by vigorous stirring to yield 5 μM solutions with different water fractions (0–90 vol%). The PL measurements of the resultant mixtures were performed immediately upon excitation at 430 nm.

Preparation of BTPEBD NPs

The procedure for BTPEBD NP fabrication consists of four steps: (i) BTPEBD (1 mg), DSPE-PEG_{2000} (1.8 mg) and DSPE-PEG_{2000}-Mal (0.2 mg) were dissolved well in THF (1 mL); (ii) after adding the obtained THF solution to water (10 mL), sonication for 2 min using a microtip sonicator at 16 W output (XL2000, Misonix Incorporated, NY) was used to afford a clear mixture; (iii) the mixture was stirred vigorously for 24 h in a fumehood to remove THF; and (iv) after filtration with a 0.2 μm syringe driven filter, the obtained BTPEBD NPs were concentrated to 0.5 mg mL^{-1} for further use.

Wide field microscopy imaging

Single BTPEBD NP fluorescence imaging was performed on a Wide-Field Microscope. The chassis is based on a Nikon ECLIPSE Ti-U inverted microscope. Light from a CW multi-line Ar ion laser (λ_{ex} = 488 nm, 10 mW output power, Melles Griot) was fiber-coupled to a Nikon Total Internal Reflection Fluorescence (TIRF) attachment and focused on the back aperture of a high numerical aperture (NA) objective (Nikon TIRF Apo, 100×, NA = 1.49, oil immersion). Immersion oil (n_D = 1.479, viscosity = 170 cS, Cargille, USA) was used for index matching. The fluorescence

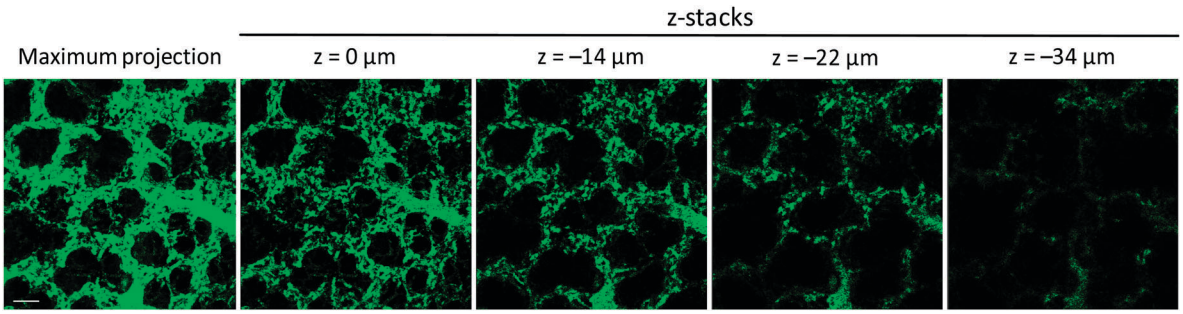

Fig. 6 Intravital two-photon fluorescence images of BTPEBD NP-stained lung vasculature at various vertical depths. The scale bar is 50 μm. The images were taken upon excitation at 800 nm with a 525/50 long-pass mirror for fluorescence collection.

emitted from the BTPEBD NPs was detected by an iXonEM + 897 EMCCD camera (512 × 512 pixels, 150 nm per pixel resolution, Andor Technology) connected to the side port of the microscope. The camera was connected to a computer furbished with camera dedicated software to control the imaging parameters, and for data acquisition. Fluorescence intensity time-traces were acquired for each frame (512 × 512 pixels, 76 × 76 μm^2) by gathering 1000 continuous frames at a frame rate of 10 Hz for 100 s. For adequate noise cancellation, the camera gain was fixed at 8 for all samples. All experiments were conducted in air under ambient conditions. The data analysis was performed using OriginPro8 software.

Cell culture

HeLa and NIH-3T3 cells were cultured at 37 °C in Dulbecco's Modified Eagle's Medium (DMEM) containing 1% penicillin-streptomycin and 10% FBS in a humidified environment containing 5% CO_2. The cells were precultured until confluence was reached prior to the experiments.

Cell imaging

HeLa cells were cultured in confocal imaging chambers at 37 °C. When the confluence reached 80%, the medium was removed and the adherent cells were washed twice with 1× PBS buffer. BTPEBD NPs (2 μM based on BTPEBD molecule) in FBS-free culture medium were added to the chamber. After incubation for 2 h, the cells were washed with 1× PBS buffer and then fixed with 4% paraformaldehyde. After staining with DAPI for 10 min, the cells were imaged by confocal laser scanning microscopy (Zeiss LSM 410, Jena, Germany) with software (Fluoview FV1000). The fluorescent signal from the BTPEBD NPs was collected from 560 to 650 nm upon excitation at 488 nm. The signal from the Hoechst 33342 channel was collected between 430 and 470 nm upon excitation at 405 nm.

Cytotoxicity study

MTT assays were used to assess the cytotoxicity of BTPEBD NPs against both cancer and normal cells. In brief, HeLa and NIH-3T3 cells were seeded in 96-well plates (Costar, IL, USA) at a density of 4×10^4 cells per mL, respectively. After 24 h incubation, the old medium was replaced by a BTPEBD NP suspension at concentrations of 12, 24, 60 and 120 μM. At 24 h post addition of BTPEBD NPs, the wells were washed with 1× PBS buffer and 100 μL of freshly prepared MTT solution (0.5 mg mL^{-1}) in culture medium was added into each well. The MTT medium solution was carefully removed after 3 h of incubation in the incubator. DMSO (100 μL) was then added into each well and the plate was gently shaken for 10 min at room temperature to dissolve all the precipitates formed. The absorbance of MTT at 570 nm was then monitored by a microplate Reader (GENios Tecan). Cell viability was expressed by the ratio of the absorbance of cells incubated with BTPEBD NPs to that of the cells incubated with culture medium only.

Intravital multiphoton imaging of the lungs

The Biological Resource Centre (BRC) Institutional Animal Care and Use Committee (IACUC) from the Agency for Science, Technology and Research (A*STAR), Singapore, is responsible for ensuring the oversight and evaluation of animal care and use programmes of an institution, and is responsible for ensuring that the care and use of the animals for scientific purposes and all animal experimental procedures are in compliance with the National Advisory Committee For Laboratory Animal Research (NACLAR) Guidelines. The experiments carried out in this study were approved by the committee and followed the NACLAR guidelines.

NACLAR has developed Guidelines which acknowledge the best practices of countries such as Australia, Canada, New Zealand, and the US, and organisations such as the Council for International Organisations of Medical Sciences (CIOMS) and the European Convention for the Protection of Vertebrate Animals Used for Experimental and Other Scientific Purposes (1986). These countries and organisations have laid down stringent guidelines and procedures governing the use and care of animals in research.

The mice were anaesthetized with a cocktail of ketamine and xylazine before cannulation of the trachea to allow connection to a mechanical ventilator (tidal volume 8–10 μL per g body weight, respiratory rate around 120 breaths per minute) (MiniVent 845; Hugo Sachs Elektronik). The mice were then placed onto a heat pad to maintain body temperature at 37 °C, followed by the removal of the skin, muscle and two rib bones to expose the lung. A custom-made vacuum window ring was used to immobilize the lung *via* application of a negative pressure vacuum (~40 mmHg). Imaging was conducted using a multiphoton LaVision TriM Scope II microscope (LaVision BioTec) equipped with a 20× 1.0 NA water immersion objective lens and a Coherent Chameleon pulsed infrared laser (Ti:Sa). To label the pulmonary vasculature, 100 μL of BTPEBD NPs were administered intravenously. The experiments were performed using an 800 nm excitation wavelength, and GFP fluorescence was detected with a 525/50 longpass mirror. 364 μm × 364 μm images were acquired at an imaging speed of 2 fps over a period of 30 minutes using a 4 μm *z*-step size with an approximate depth of 20 μm. After acquisition, 24 frames were averaged to match respiratory movements and drifts during imaging were corrected where necessary using FIJI. Images were subsequently transformed into time series movies using Imaris. FIJI was used to measure the fluorescence intensity of the BTPEBD NPs at 20 independent locations in the vasculature.

Synthesis of 1-(4-(4,4,5,5-tetramethyl-1,3,2-dioxaborolan-2-yl)phenyl)-1,2,2-triphenylethylene (1)

To a mixture of 1-(4-bromophenyl)-1,2,2-triphenylethylene (1.00 g, 2.44 mmol), potassium acetate (0.84 g, 8.54 mmol), bis(pinacolato)diboron (0.93 g, 3.66 mmol) and $Pd(dppf)Cl_2$ (88 mg, 0.12 mmol) was added anhydrous dioxane (15 mL). The reaction mixture was stirred under an argon atmosphere at 85 °C for 20 h. After cooling down to room temperature, the

mixture was subsequently diluted with dichloromethane (50 mL), washed with water (50 mL × 3) and dried over $MgSO_4$. After removing the solvents under reduced pressure, the residue was purified by silica gel column chromatography (hexane/dichloromethane = 7/3, v/v) to afford **1** as a white solid (1.05 g, yield: 95%). ^{1}H NMR (600 MHz, $CDCl_3$, ppm) δ: 7.55 (d, J = 6 Hz, 2H), 7.09 (m, 9H), 7.05–6.99 (m, 8H), 1.32 (s, 12H).

Synthesis of 4,7-bis[4-(1,2,2-triphenylvinyl)phenyl]benzoxadiazole (DTPEBD)

A Schlenk tube was charged with **1** (192.3 mg, 0.42 mmol), 4,7-dibromo-2,1,3-benzoxadiazole (50.0 mg, 0.18 mmol), $Pd(PPh_3)_4$ (10.7 mg, 9 μmol), potassium carbonate (244.8 mg, 1.8 mmol), tetrabutylammonium bromide (7.8 mg, 24 μmol), water (0.9 mL) and toluene (20 mL). The reaction mixture was kept at 90 °C for 2 days under an argon atmosphere. After the reaction mixture was cooled down to room temperature, it was sequentially diluted with dichloromethane (100 mL), washed with water (50 mL × 3) and dried over $MgSO_4$. After solvent removal, the residue was purified by silica gel column chromatography (hexane/dichloromethane = 9/2, v/v) to afford DTPEBD as a bright green solid (130.5 mg, yield: 93%). ^{1}H NMR (600 MHz, $CDCl_3$, ppm) δ: 7.82 (d, J = 12 Hz, 4H), 7.60 (s, 2H), 7.19 (d, J = 6 Hz, 4H), 7.15–7.08 (m, 22H), 7.08 (m, 4H), 7.06–7.04 (m, 4H). ^{13}C NMR (150 MHz, $CDCl_3$, ppm) δ: 149.28, 144.92, 143.73, 143.66, 143.61, 141.93, 140.37, 133.17, 132.06, 131.56, 131.49, 131.47, 128.34, 128.27, 128.00, 127.92, 127.81, 127.63, 126.86, 126.75, 126.71.

Conclusions

In summary, fluorescent organic NPs based on BTPEBD with aggregation-induced emission characteristics were developed for cellular imaging and real-time two-photon Lung vasculature imaging. Compared to other reported long wavelength emissive AIE molecules, BTPEBD can be readily synthesized from commercially available starting materials *via* two steps in high yields, which is of vital importance for practical applications. The obtained BTPEBD NPs exhibit large Stokes shift (>135 nm), ultrahigh quantum yield (>90%) in water and good biocompatibility. Furthermore, the high brightness and good photostability of the BTPEBD NPs have been demonstrated at a single NP level. The *in vitro* cell imaging and *in vivo* two-photon lung vasculature imaging results proved the BTPEBD NPs to be excellent fluorescent contrast agents for bioimaging applications.

Conflicts of interest

There are no conflicts to declare.

Acknowledgements

The authors are grateful to the Singapore National Research Foundation (R279-000-444-281 and R279-000-483-281) and the National University of Singapore (R279-000-482-133) for financial support.

Notes and references

1 A. Reisch and A. S. Klymchenko, *Small*, 2016, **12**, 1968–1992.
2 E. C. Cho, C. Glaus, J. Chen, M. J. Welch and Y. Xia, *Trends Mol. Med.*, 2010, **16**, 561–573.
3 M. Chen and M. Yin, *Prog. Polym. Sci.*, 2014, **39**, 365–395.
4 A. M. Smith, H. Duan, A. M. Mohs and S. Nie, *Adv. Drug Delivery Rev.*, 2008, **60**, 1226–1240.
5 F. Wang and X. Liu, *Chem. Soc. Rev.*, 2009, **38**, 976–989.
6 L. Wang, W. Zhao and W. Tan, *Nano Res.*, 2008, **1**, 99–115.
7 J. P. Wilcoxon and B. L. Abrams, *Chem. Soc. Rev.*, 2006, **35**, 1162–1194.
8 K. Li and B. Liu, *Chem. Soc. Rev.*, 2014, **43**, 6570–6597.
9 S. N. Baker and G. A. Baker, *Angew. Chem., Int. Ed.*, 2010, **49**, 6726–6744.
10 S. Santra, D. Dutta, G. A. Walter and B. M. Moudgil, *Technol. Cancer Res. Treat.*, 2005, **4**, 593–602.
11 J. B. Birks, *Photophysics of Aromatic Molecules*, Wiley, London, 1970.
12 J. Mei, Y. Hong, J. W. Y. Lam, A. Qin, Y. Tang and B. Z. Tang, *Adv. Mater.*, 2014, **26**, 5429–5479.
13 J. Mei, N. L. C. Leung, R. T. K. Kwok, J. W. Y. Lam and B. Z. Tang, *Chem. Rev.*, 2015, **115**, 11718–11940.
14 D. Ding, K. Li, B. Liu and B. Z. Tang, *Acc. Chem. Res.*, 2013, **46**, 2441–2453.
15 K. Li and B. Liu, *Chem. Soc. Rev.*, 2014, **43**, 6570.
16 K. Li, W. Qin, D. Ding, N. Tomczak, J. Geng, R. Liu, J. Liu, X. Zhang, H. Liu and B. Liu, *Sci. Rep.*, 2013, **3**, 1150.
17 J. Geng, J. Liu, J. Liang, H. Shi and B. Liu, *Nanoscale*, 2013, **5**, 8593.
18 K. Li, Z. Zhu, P. Cai, R. Liu, T. Nikodem, D. Ding, J. Liu, W. Qin, Z. Zhao, Y. Hu, X. Chen, B. Z. Tang and B. Liu, *Chem. Mater.*, 2013, **25**, 4181–4187.
19 D. Ding, D. Mao, K. Li, X. Wang, W. Qin, R. Liu, D. S. Chiam, N. Tomczak, Z. Yang and B. Z. Tang, *ACS Nano*, 2014, **8**, 12620–12631.
20 J. Zhang, C. Li, X. Zhang, S. Huo, S. Jin, F.-F. An, X. Wang, X. Xue, C. I. Okeke, G. Duan, F. Guo, X. Zhang, J. Hao, P. C. Wang, J. Zhang and X.-J. Liang, *Biomaterials*, 2015, **42**, 103–111.
21 W. Qin, D. Ding, J. Z. Liu, W. Z. Yuan, Y. Hu, B. Liu and B. Z. Tang, *Adv. Funct. Mater.*, 2012, **22**, 771–779.
22 Z. Song, D. Mao, S. H. P. Sung, R. T. K. Kwok, J. W. Y. Lam, D. Kong, D. Ding and B. Z. Tang, *Adv. Mater.*, 2016, **28**, 7249–7256.
23 Y. Huang, P. Zhang, M. Gao, F. Zeng, A. Qin, S. Wu and B. Z. Tang, *Chem. Commun.*, 2016, **52**, 7288–7291.
24 R. Hu, C. Yang, Y. Wang, G. Lin, W. Qin, Q. Ouyang, W.-C. Law, Q. T. Nguyen, H. S. Yoon, X. Wang, K.-T. Yong and B. Z. Tang, *Nano Res.*, 2015, **8**, 1563–1576.
25 J. Geng, K. Li, W. Qin, B. Z. Tang and B. Liu, *Part. Part. Syst. Charact.*, 2014, **31**, 1238–1243.
26 J. Geng, Z. Zhu, W. Qin, L. Ma, Y. Hu, G. G. Gurzadyan, B. Z. Tang and B. Liu, *Nanoscale*, 2014, **6**, 939–945.
27 D. Ding, K. Li, W. Qin, R. Zhan, Y. Hu, J. Liu, B. Z. Tang and B. Liu, *Adv. Healthcare Mater.*, 2013, **2**, 500–507.

28 H. Shi, N. Zhao, D. Ding, J. Liang, B. Z. Tang and B. Liu, *Org. Biomol. Chem.*, 2013, **11**, 7289–7296.
29 J. Liu, C. Chen, S. Ji, Q. Liu, D. Ding, D. Zhao and B. Liu, *Chem. Sci.*, 2017, **8**, 2782–2789.
30 D. Ding, C. C. Goh, G. Feng, Z. Zhao, J. Liu, R. Liu, N. Tomczak, J. Geng, B. Z. Tang, L. G. Ng and B. Liu, *Adv. Mater.*, 2013, **25**, 6083–6088.
31 A. Ding, H. Hao, Y. Gao, Y. Shi, Q. Tang and Z. Lu, *J. Mater. Chem. C*, 2016, **4**, 5379–5389.
32 Y. Gao, G. Feng, T. Jiang, C. C. Goh, L. G. Ng, B. Liu, B. Li, L. Yang, J. Hua and H. Tian, *Adv. Funct. Mater.*, 2015, **25**, 2857–2866.
33 Q. Ye, S. Chen, D. Zhu, X. Lu and Q. Lu, *J. Mater. Chem. B*, 2015, **3**, 3091–3097.
34 J. Geng, K. Li, D. Ding, X. H. Zhang, W. Qin, J. Z. Liu, B. Z. Tang and B. Liu, *Small*, 2012, **8**, 3655–3663.
35 Y. Wang, M. Chen, N. Alifu, S. Lo, W. Qin, A. Qin, B. Z. Tang and J. Qian, *ACS Nano*, 2017, **11**, 10452–10461.
36 Z. Zhu, J. Qian, X. Zhao, W. Qin, R. Hu, H. Zhang, D. Li, Z. Xu, B. Z. Tang and S. He, *ACS Nano*, 2016, **10**, 588–597.
37 Z. Zhu, C. W. T. Leung, X. Zhao, Y. Wang, J. Qian, B. Z. Tang and S. He, *Sci. Rep.*, 2015, **5**, 15189.
38 J. Geng, C. C. Goh, W. Qin, R. Liu, N. Tomczak, L. G. Ng, B. Z. Tang and B. Liu, *Chem. Commun.*, 2015, **51**, 13416–13419.
39 S. M. A. Fateminia, Z. Wang, C. C. Goh, P. N. Manghnani, W. Wu, D. Mao, L. G. Ng, Z. Zhao, B. Z. Tang and B. Liu, *Adv. Mater.*, 2017, **29**, 1604100.
40 Q. Zhao, K. Li, S. Chen, A. Qin, D. Ding, S. Zhang, Y. Liu, B. Liu, J. Z. Sun and B. Z. Tang, *J. Mater. Chem.*, 2012, **22**, 15128–15135.
41 J. Zhang, R. Chen, Z. Zhu, C. Adachi, X. Zhang and C.-S. Lee, *ACS Appl. Mater. Interfaces*, 2015, **7**, 26266–26274.
42 H. Lu, Y. Zheng, X. Zhao, L. Wang, S. Ma, X. Han, B. Xu, W. Tian and H. Gao, *Angew. Chem., Int. Ed.*, 2016, **55**, 155–159.
43 Z. Wang, L. Yan, L. Zhang, Y. Chen, H. Li, J. Zhang, Y. Zhang, X. Li, B. Xu and X. Fu, *Polym. Chem.*, 2014, **5**, 7013–7020.
44 W. Qin, K. Li, G. Feng, M. Li, Z. Yang, B. Liu and B. Z. Tang, *Adv. Funct. Mater.*, 2014, **24**, 635–643.
45 T. Santa, *Biomed. Chromatogr.*, 2014, **28**, 760–766.
46 J. Bouffard and T. M. Swager, *Macromolecules*, 2008, **41**, 5559–5562.
47 J. Liu, D. Ding, J. Geng and B. Liu, *Polym. Chem.*, 2012, **3**, 1567–1575.
48 J. Liu, G. Feng, R. Liu, N. Tomczak, L. Ma, G. G. Gurzadyan and B. Liu, *Small*, 2014, **10**, 3110–3118.
49 J. Liu, J. Geng and B. Liu, *Chem. Commun.*, 2013, **49**, 1491–1493.
50 R. Hu, E. Lager, A. Aguilar-Aguilar, J. Liu, J. W. Lam, H. Sung, I. D. Williams, Y. Zhang, K. S. Wong and E. Pena-Cabrera, *J. Phys. Chem. C*, 2009, **113**, 15845–15853.
51 J. M. Drake, M. L. Lesiecki and D. M. Camaioni, *Chem. Phys. Lett.*, 1985, **113**, 2887.

